Dyes and Pigments 142 (2017) 491–498

Contents lists available at ScienceDirect

Dyes and Pigments

journal homepage: www.elsevier.com/locate/dyepig

Highly efficient Far Red/Near-Infrared fluorophores with aggregation-induced emission for bioimaging

Fengli Zhang [a], Yizeng Di [a], Yue Li [b], Qingkai Qi [a], Jingyu Qian [a], Xueqi Fu [b], Bin Xu [a, **], Wenjing Tian [a, *]

[a] State Key Laboratory of Supramolecular Structure and Materials, Jilin University, Changchun, 130012, PR China
[b] College of Life Sciences, Jilin University, Changchun, 130012, PR China

ARTICLE INFO

Article history:
Received 16 January 2017
Received in revised form
1 April 2017
Accepted 2 April 2017
Available online 8 April 2017

Keywords:
Aggregation-induced emission
Tetraphenylethene derivatives
Biocompatible dye
Bioimaging
Far Red/Near-Infrared
Fluorescent compounds

ABSTRACT

Organic fluorescent probes play an important role in modern biomedical research, such as biological sensing and imaging. However, the development of organic fluorophores with efficient aggregate state emissions expanded to the red to near-infrared region is still challenging. Here, we present a series of highly efficient Far Red/Near-Infrared (FR/NIR) fluorescent compounds with aggregation-induced emission (AIE) properties by attaching electron donor and accepter to tetraphenylethene (TPE) moieties through a simple synthesis method. These compounds exhibited the pronounced fluorescence enhancement in aggregate state, the red to near infrared emission, and can be facilely fabricated into uniform compounds-loaded Pluronic F127 NPs. The emission maximum of the NPs fabricated by the self-assembly method is in the range of 550–850 nm and the highest fluorescent quantum yield can get to 15.2%. The biological imaging of NPs of compound **1** and **2** for A549 lung cancer cell indicates that these compounds are effective fluorescent probes for cancer cells with high specificity, high photostability and good fluorescence contrast.

1. Introduction

Fluorescent probes have attracted extensive attentions due to their imaging of biological species and monitoring ability of the life process [1,2]. Among various fluorescent probes, inorganic semiconductor quantum dots (QDs) have been widely used because of their unique optical and electronic properties, *i.e.* size-tunable light emission, superior signal brightness, resistance to photo bleaching, and broad absorption spectra for simultaneous excitation of multiple fluorescence colors [3]. Whereas, QDs induce notorious cytotoxicity owing to the release of heavy metal ions, especially in anoxidative environment, which limited their applications in some fields of biological imaging [4,5]. In comparison with QDs, organic dye-loaded fluorescent nanoparticles (NPs) have exhibited superior cytocompatibility and fluorescence stability [6]. However, conventional organic dye may suffers weakened or annihilated fluorescence in nanoparticles matrices due to the planar aromatic structure which can lead to non-radiative process *via* π–π stacking or upon interaction with bioanalyses, which is the so-called aggregation-caused quenching (ACQ) effect [7–10]. In 2001, Tang et al. reported a series of silole derivatives which were non-emissive in dilute solutions but exhibited strong luminescence when the molecules were aggregated in concentrated solutions or casted into solid films due to the restriction of intramolecular rotation [11–13]. That is aggregation-induced emission (AIE).

Recently, many AIE fluorophores with highly twisted structures have been synthesized and their various applications have been explored, especially in optoelectronic and biological areas [12–18]. TPE is one of the typical AIEgens. Most of the TPE derivatives give blue or green emission, limited their applications for bioimaging [12,19–33]. Meanwhile, far FR/NIR fluorophores play a crucial role in fluorescent bioimaging because of their low tissue absorption and weak tissue auto fluorescence in FR/NIR region, thus can minimize the background interference and improve the image sensitivity [34–39]. Tang et al. reported a series of AIE fluorophores by conjugating a common AIE molecule with ACQ red fluorophores, emitted fluorescence in the FR/NIR region and assembled into nanoparticles for vitro bioimaging of cancer cells [10,19,33,40,41].

Herein, we designed and synthesized FR/NIR AIE fluorophores by selecting proper combination of electron donor (D) and acceptor

* Corresponding author.
** Corresponding author.
E-mail addresses: xubin@jlu.edu.cn (B. Xu), wjtian@jlu.edu.cn (W. Tian).

http://dx.doi.org/10.1016/j.dyepig.2017.04.004
0143-7208/

(A) to create FR/NIR fluorophores. By introducing the dimethylamine and cyano moieties into TPE, four novel FR/NIR fluorescent compounds **1, 2, 3** and **4** with distinct AIE characteristics have been synthesized. The highest quantum yield of the four compounds in solid state can reach to 40%. These compounds were easily fabricated into uniform compound-loaded NPs. Remarkably, compound **1**-loaded Pluronic F127 NPs showed the long emission wavelength at the peak of 650 nm and high fluorescence quantum yield of 15.2%. The biological imaging of NPs of compound **1** and **2** for A549 lung cancer cell indicates that these compounds are effective fluorescent probes for cancer cells.

2. Experimental section

2.1. Materials

Tetrahydrofuran (THF) was distilled from sodium benzophenoneketyl under nitrogen immediately prior to use. And all the other chemicals were purchased from Aladdin and used as received without further purification.

2.2. Instruments

^{1}H NMR spectra were recorded on a 500 MHz Bruker Avance, using DMSO as solvent. ^{13}C NMR spectra were recorded on a 125 MHz Bruker Avancespectrometer, using $CDCl_3$ as a solvent and TMS as an internal standard ($\delta = 0.00$ ppm). LC-HRMS was obtained by Agilent 1290-microTOF Q II. Element analyses were performed on a FlashEA1112 spectrometer. GCMS were recorded on a Thermo Fisher ITQ1100. UV/Vis spectra were measured on a Shimadzu UV-2550 spectrophotometer. Fluorescence spectra were recorded by Shimadzu RF-5301 PC spectrometer and Maya2000Pro optical fiber spectrophotometer. Solid photoluminescence (PL) efficiencies were measured by using an integrating sphere (C-701, Labsphere Inc.), with 365 and 470 nm Ocean Optics LLS-LED as the excitation source, and the light was introduced into the integrating sphere through optical fiber. The confocal laser scanning microscopy images were obtained on an Olympus FV1000 confocal laser scanning microscope.

2.3. Synthesis

Under N_2 atmosphere, a three-necked flask equipped with a magnetic stirrer was charged with zinc powder (4.2 g, 65 mmol) and 40 mL THF. The mixture was cooled to −5–0 °C, and $TiCl_4$ (3.6 mL, 32.4 mmol) was slowly added by a syringe with the temperature kept under 10 °C. The suspending mixture was warmed to room temperature and stirred for 0.5 h, then heated at reflux for 2.5 h. The mixture was again cooled to −5–0 °C, charged with pyridine (0.24 mL, 3 mmol) and stirred for 10 min. The solution of two carbonyl compounds (in 6:6 mmol to 6:7.2 mmol mole ratios, in 15 mLTHF) was added slowly. After addition, the reaction mixture was heated at reflux until the carbonyl compounds were consumed (monitored by TLC). The reaction was quenched with 10% Na_2CO_3 aqueous solution and taken up with CH_2Cl_2. The organic layer was collected and concentrated. The crude material was purified by flash chromatography to give the desired products.

The 1-(4-bromophenyl)-1,2,2-triphenylethylene was solved in THF, the added n-BuLi at −78 °C for 2 h, followed by addition of dimethylformamide, the crude material was kept at room temperature for 2 h. The mixture was quenched by water and purified by flash chromatography, gave the expected aldehyde.

Knoevenagel reaction was taking place between the aldehyde and the cyano derivative under alkaline conditions. The mixture was purified by flash chromatography, gave the target molecular.

2.4. Preparation of fluorogen-loaded F-127 NPs

The fluorogen-loaded F-127 NPs were prepared by using the self-assembly method as described previously for conjugated polymers [38]. In THF solution (3 mL) containing F-127 (200 mg), TPE derivatives (from 0.25 to 2 mg) was poured into water (10 mL). And then the mixture was evaporated to completely remove the organic agent (THF) by nitrogen purge. The NP suspension was further purified with a 0.2 mm syringe filter to obtain fluorogen-loaded F-127 NPs.

2.5. Cell culture

The A-549 cell line was maintained in DMEM (Gibco) supplemented with 10% FBS (Gibco), and 100 U/mL of penicillin under a humidified atmosphere containing 95% air and 5% CO_2 at 37 °C. The cells were precultured until confluence was reached prior to experiments. The cells were harvested by briefly rinsing with culture media followed by incubation with trypsin-EDTA solution (0.25% w/v trypsin, 0.53 mM EDTA) for cell imaging.

2.6. Cell viability and cytotoxicity using an MTT assay

We determined the cytotoxic effects of F-127 dots on A549 cells and the cell viability of A549 using an MTT assay. A549 cells need to be incubated with F-127 dots in the dark for 24 h before interacting with MTT assay. After incubation, a sample of 100 μL of MTT (5 mg/ml) in phosphate buffer solution (PBS) was added to each well of a 96-well plate and cultured for 4 h at 37 °C. After removing the medium containing MTT, 150 μL of warm dimethyl sulfoxide (DMSO) was added to each well to dissolve the formazan. The samples were shaken for 10 min at room temperature in the dark. The absorbance was read at 490 nm using a microplate reader. Percentage cell viability and cytotoxicity were calculated from the following formulas: Percentage cell viability = (average Abs. value of experimental group − average Abs. value of blank group)/(average Abs. value of control group − average Abs. value of blank group) × 100%; percentage cell cytotoxicity = [1 − (average Abs value of experimental group − average Abs value of blank group)/(average Abs value of control group − average Abs value of blank group)] × 100%; percentage cell cytotoxicity = (1 − Percentage cell viability) × 100%.

2.7. Cell imaging

A million A549 cells in 100 mL labeling buffer (PBS containing 1% BSA and 2 mM EDTA) were incubated with F-127 dots for 4 h. After washing two times, cell suspension was dropwise to a coverslip, then covered with a glass slide and imaged immediately under confocal laser scanning microscope.

2.8. Determination of quantum yields

By using rhodamine B as the reference (fluorescence quantum yield equal to 0.69 in dilute ethanol solution with excitation wavelength of 365 nm), the fluorescence quantum yield of the near-infrared emission dots were measured according to the following equation.

$$\eta_s = \eta_r \left(\frac{A_r}{A_s}\right)\left(\frac{I_s}{I_r}\right)\left(\frac{n_r^2}{n_s^2}\right)$$

where η_r is the quantum yield of reference, A_r is the absorbance of reference at the excitation wavelength, A_s is the absorbance of sample at the excitation wavelength, I_r is the area under the emission peak on a wavelength scale of reference, I_s is the area

under the emission peak on a wavelength scale of sample, n_r is the refractive index of the reference solvent, n_s is the refractive index of the sample solvent. Absorption spectrum and emission spectrum measured by the Maya 2000 pro fiber spectrometer (Ocean Optics). Solid state PL efficiencies were measured by using an integrating sphere (C-701, Labsphere Inc.) with a 365 nm Ocean Optics LLS-LED as the excitation source, and the laser was introduced into the sphere through the optical fiber.

3. Result and discussion

3.1. Synthesis and characterizations

Compound **1**, **2**, **3** and **4** were synthesized by a series of chemical reactions according to Scheme 1. The detailed synthetic procedure and characterizations are described in the Experimental Section and Supporting Information.

3.2. Optical properties

The UV-vis absorption (solid lines) and normalized PL spectra (dashed lines) of compound **1, 2, 3** and **4** are shown in Fig. 1. Each compound has a high absorption peak at around 330 nm, which is attributed to π–π* transition, and a weak absorption ranging from 440 to 490 nm, which represents the intramolecular charge transfer (ICT) transition between dimethylamine and cyano moieties. The emission peak of the compounds ranged from red to the NIR region with large Stokes shifts, which facilitates to improve the signal/background ratios of fluorescent images by avoiding imaging interference between the emission and excitation. Compound **1** exhibited high solid state FR/NIR emission with excellent quantum yields of 0.40 measured by an integrating sphere (C-701, Labsphere Inc.).

In order to better understand the ICT transitions of these fluorophores, we performed density functional theory (DFT) calculations for compound **1**–**4** by using Gaussian 09/B3LYP/6-31G(d). As shown in Fig. 2, the molecular orbital density of the Highest Occupied Molecular Orbital (HOMO) is mainly located in the central tetraphenylethene and dimethylamine moieties. The Lowest Unoccupied Molecular Orbital (LUMO) level is primarily localized in cyan group, which suggests a strong intramolecular charge transfer between dimethylamine and cyano moieties within the compounds, leading to the FR/NIR emission.

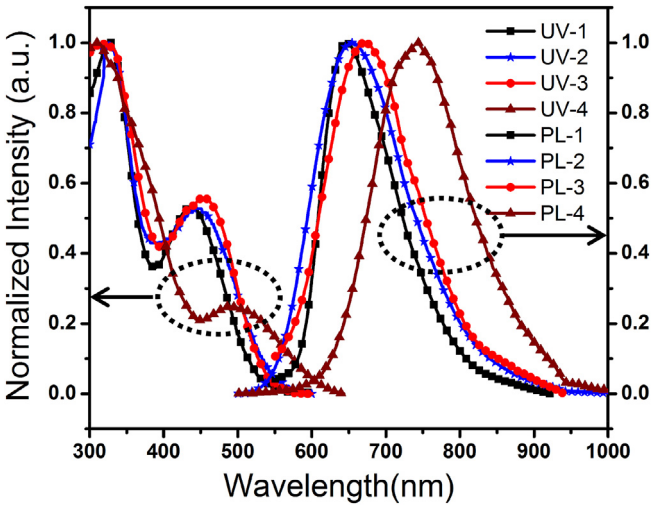

Fig. 1. UV-vis absorption and normalized photoluminescence spectra of 10 mM of each compound **1, 2, 3** and **4** in THF/water (v/v = 1/9).

The four compounds exhibited remarkable AIE properties. For example, compound **1** was almost non-emissive in THF. As shown in Fig. 3, in dilute THF solution, compound **1** exhibited weak fluorescence. When f_w (volume fraction of water) varied from 0 to 50%, the PL spectra of the solutions changed little. When f_w was 60% or higher, PL intensity and fluorescence quantum yield both increased evidently. When the water fraction was increased to 90%, the PL

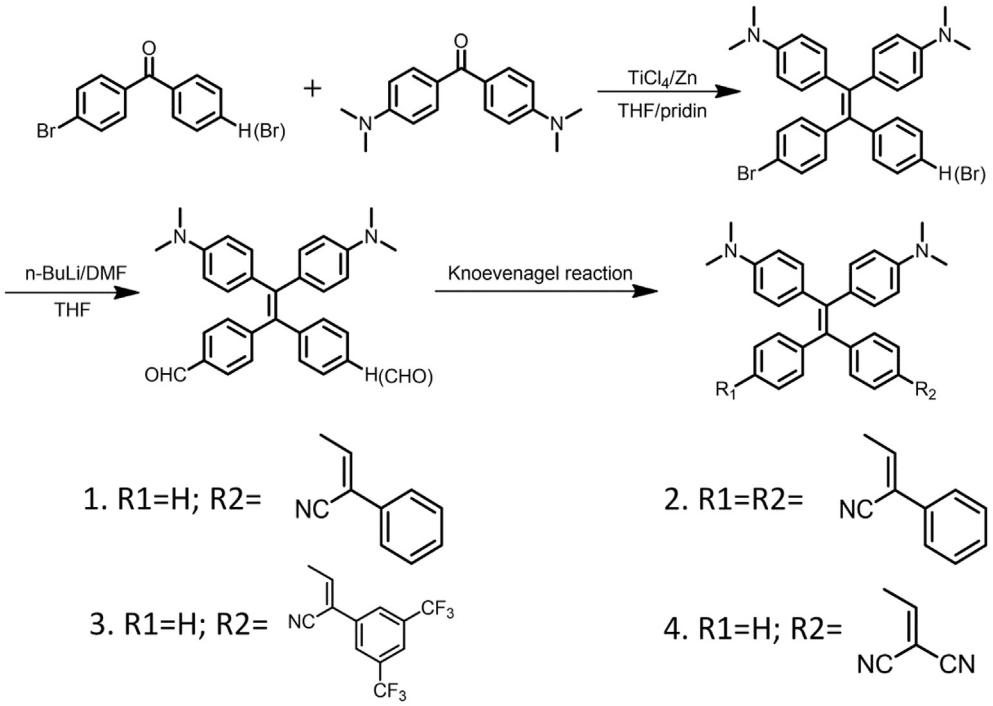

Scheme 1. The synthetic route of TPE derivatives.

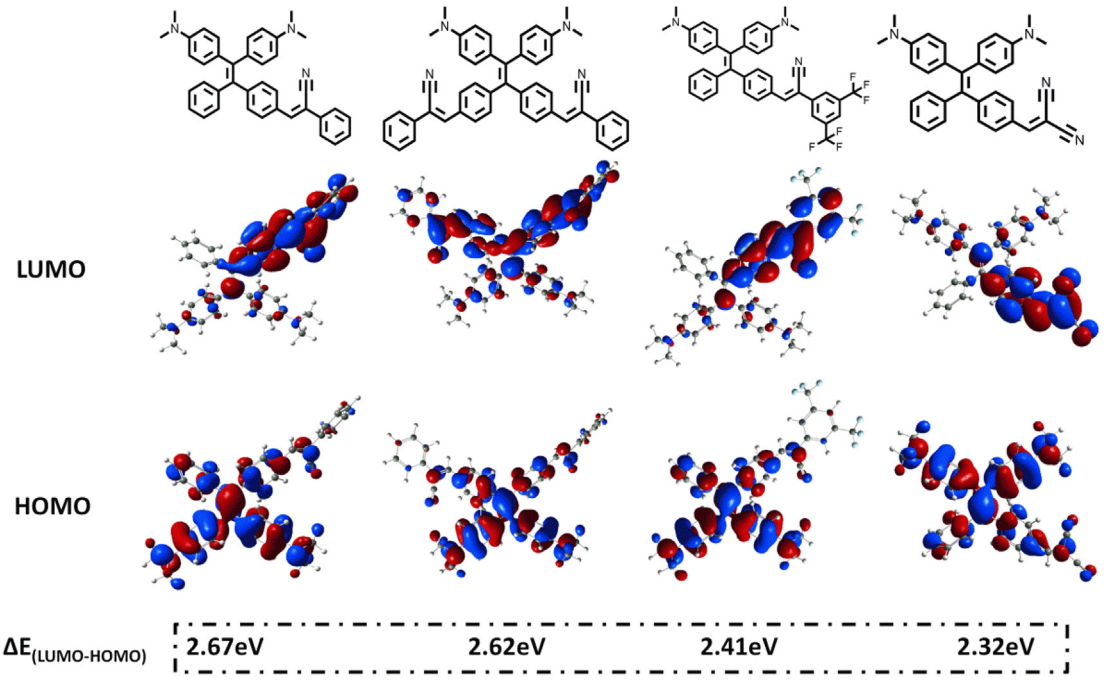

Fig. 2. Chemical structures and HOMO–LUMO distributions of the compound **1, 2, 3** and **4** optimized structures of the HOMO and LUMO were calculated by TD-DFT (Gaussian 09/B3LYP/6-31G(d)).

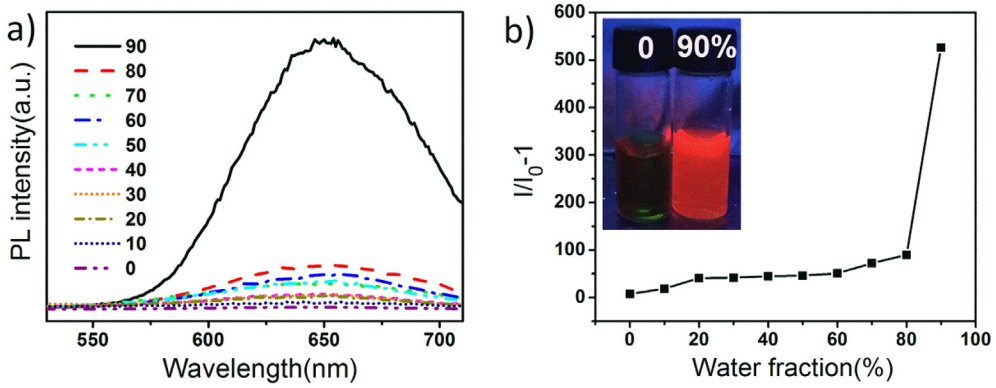

Fig. 3. (a) PL spectra of **1** in THF/water mixtures with different water fractions (f_w). (b) Plot of peak intensity of **1** versus water fraction in the aqueous mixtures. [**1**] = 10×10^{-6} M, λ_{ex} = 365 nm.

intensity was about 550 times greater than that in pure THF. The enhancements were ascribed to aggregation formation, which were induced by the addition of water. In aggregates, the propeller shape of compound **1** packed closely, leading to the restriction of the rotations of phenyls in TPE units, which is the progress that exhausts the excited energy and renders it non-radiative. The emission maximum for the aggregates of compound **1** is at 650 nm, while the PL spectrum ranges from 570 to 860 nm, covered a rather large area in NIR region. Compounds **2**–**4** show similar properties as compound **1** (see Figs. S1–3). The FR/NIR emission and desirable fluorescence quantum yield suggest these molecules can be used as potential fluorescent probes for bioimaging.

3.3. Nanoparticle preparation and characterization

In order to apply these compounds as the biosensors in living tissue cells, we prepared organic fluorescent AIE nanoparticles (NPs) through a modified nanoprecipitation method by using F-127 as the encapsulation matrix. A THF solution (3 mL) containing compound **1** (0.25–2 mg) and F-127 (fixed at 200 mg) was injected slowly into water (10 mL). Compound **1** was aggregated and entangled within the hydrophobic domains of the F-127 chains, accompanied its hybridization with the hydrophobic fluorogen. And then the mixture was evaporated to completely remove the organic agent (THF) by nitrogen purge. During compound **1**-loaded F-127 NPs formation, the hydrophobic units of F-127 molecule tended to locate inside the NPs while the hydrophilic units localized on the surface of the NPs in the aqueous environment. Transmission electron microscopy (TEM) images of the compound **1** loaded F-127 NPs with 1 mg of compound **1** are shown in Fig. 4 as an example. The images indicate that the AIE-active fluorogen-loaded NPs had a spherical shape and a smooth surface with an almost uniform size of around 30 nm. All the F-127 NPs loaded variable fluorogen have a narrow particle size distribution around 35–40 nm (see Figs. S7–9).

Table 1 shows the fluorescence quantum yield of the compound

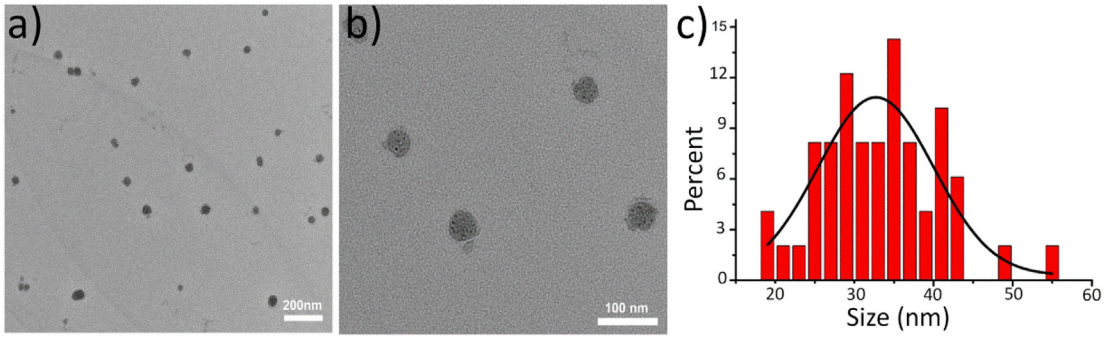

Fig. 4. (a–b) TEM images of **1**@F-127 NPs in different magnifications. (c) Diameter statistics of NPs *via* the counting of the NPs in the TEM images. More than 100 NPs were counted.

Table 1
Fluorescence quantum yield of compound **1** in different weight loaded F-127 NPs.

Compound **1** loading weight (mg)	Pluronic F-127 loading weight (mg)	Fluorescent quantum yield (%)
0.25	200	4.52
0.50	200	5.64
0.75	200	5.84
1.00	200	7.09
1.25	200	10.8
1.5	200	15.2
1.75	200	14.7
2.00	200	14.6

1 loaded F-127 NPs prepared at different weight of compound **1**. The fluorescence quantum yield values of the **1**-loaded F-127 NPs in water were measured using Rhodamine B in ethanol as the standard. The fluorescence quantum yield initially increased and then decreased with increasing the amount of compound **1**. It eventually reached a value of 15.2% at a compound **1** loaded weight of 1.5 mg. Therefore, in order to obtain the best fluorescence imaging result, the NPs were prepared by using a precursor solution with the proper mass ratio of 200: 1.5 (F-127: compound **1**). The quantum yield also reached to 6.4%, 5.7%, and 4.3% for compound **2**–**4,** respectively (see Figs. S4–6).

Excellent fluorescence stability in aqueous media is essential for biological applications, especially in long-term studies. The fluorescence intensity evolution of compound **1** and **2** loaded F-127 NPs was investigated by monitoring their fluorescence changes upon incubation in a phosphate buffer solution (PBS) under different incubation time. As shown in Fig. 5a and its inset, no obvious

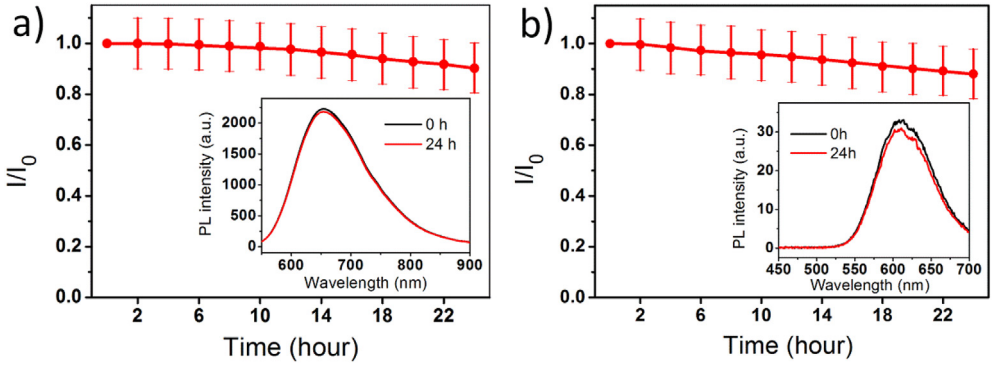

Fig. 5. PL intensity evolution of compound **1** loaded F-127 NPs (a) and compound **2** loaded F-127 NPs (b) upon continuous excitation at 405 nm (0.5 mW) following the incubation time until 24 h. I_0 is the initial fluorescence intensity and I is the fluorescence intensity of the sample after continuous exposure for designed time intervals.

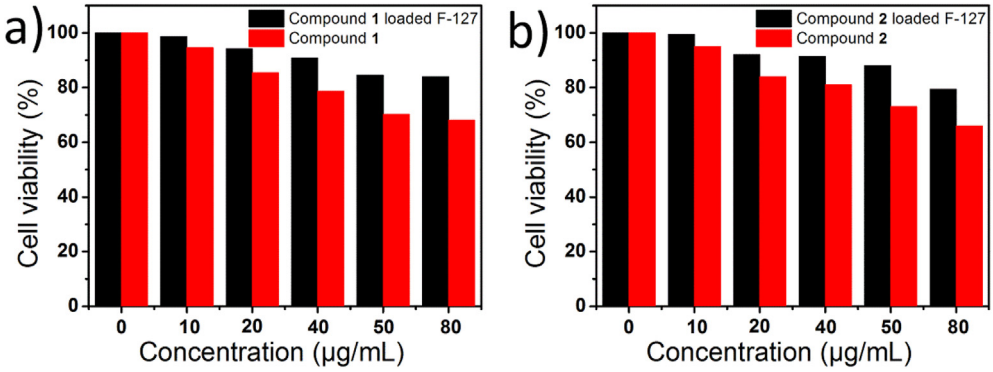

Fig. 6. Metabolic viability of A549 cancer cells after incubation with compound **1** and **2** loaded F-127 NPs and compound **1** and compound **2** at various fluorogen concentration for 24 h.

decrease of the fluorescence intensity was observed after excitation at 405 nm (0.5 mW) for 24 h, which suggests the well stability of the prepared NPs. Thus, the excellent optical properties of the NPs, such as near-infrared emission, large Stokes shift, high fluorescent quantum yield and good photostability make them suitable candidates for bioimaging.

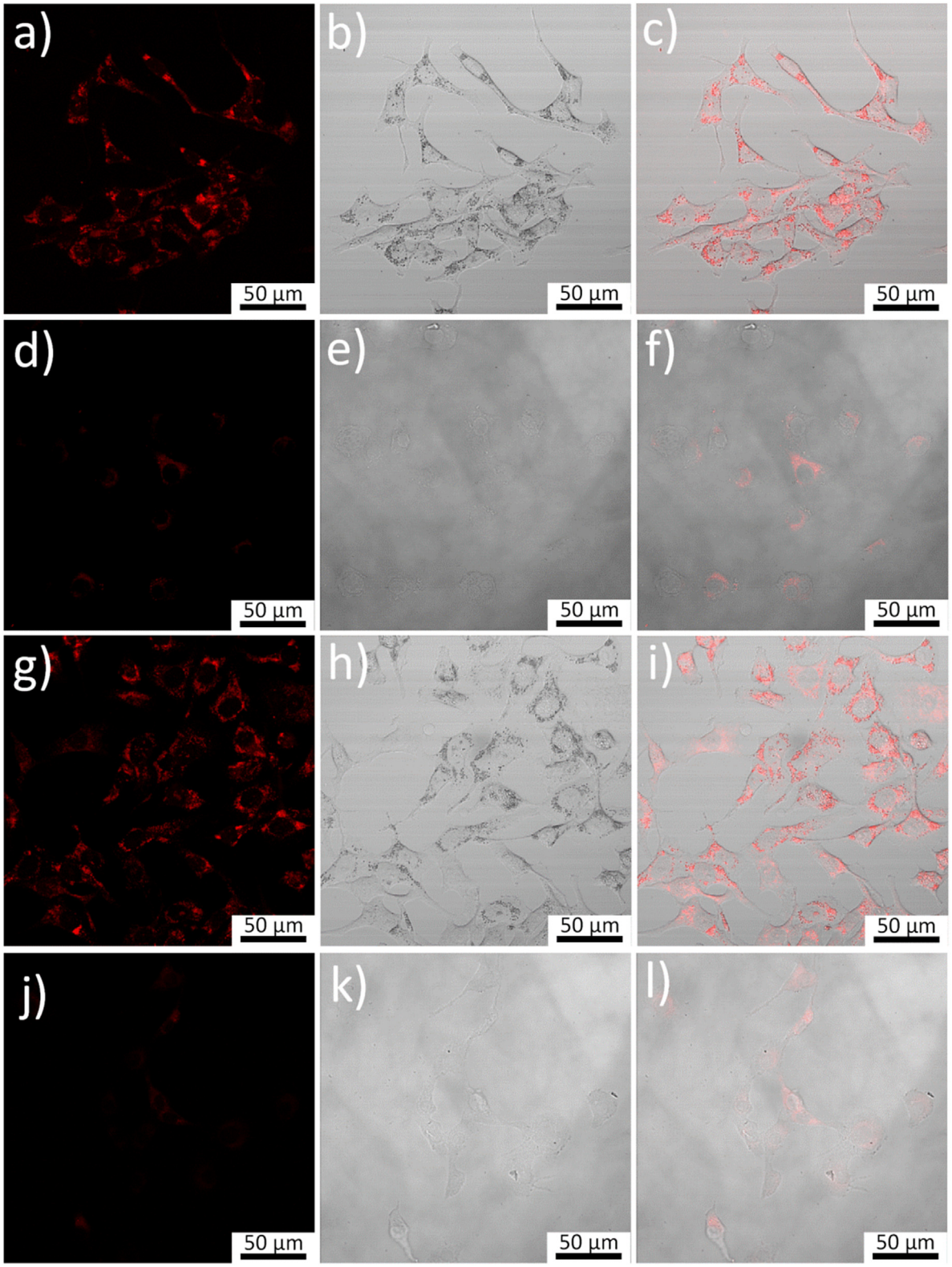

Fig. 7. Confocal fluorescence images of F-127 NPs for A549 and NIH/3T3; (a)–(c) compound **1** loaded F-127 NPs for A549; (d)–(f) compound **1** loaded F-127 NPs for NIH/3T3. (g)–(i) compound **2** loaded F-127 NPs for A549; (j)–(l) compound **2** loaded F-127 NPs for NIH/3T3; (a)–(l) were incubated for 3 h. Incubation concentration of NPs was 30 μg/mL. Excitation light: 405 nm.

3.4. Cytotoxicity

We took compound **1** and **2** loaded F-127 NPs as examples to investigate the toxicity. The cytotoxicity was evaluated with A549 cells through MTT assay. First, cancer cells were seeded in 96-well plates (10^4 cells per mL) and incubated for 24 h. Then, various concentrations of fluorogen-loaded F-127 NPs were added into the 96-well plate, and the cells with the NPs were incubated at 37 °C. After 24 h, 100 μL of MTT solution (5 mg mL^{-1} in PBS) was added into each well and incubated for 4 h. 100 μL of DMSO were added into each well and the plate was gently shaken for 5 min at room temperature to dissolve the internalized purple formazan crystals. The absorbance at 570 nm was measured with a microplate reader (Thermo Varioskan Flash). The result was expressed as a percentage of the absorbance of the blank control. Every experiment was performed for at least three times [28]. Cell viability was expressed by the ratio of the absorbance of the cells incubated with compound **1** and **2** loaded F-127 NPs suspension to that of the cells incubated with culture medium only. Fig. 6 shows the cytotoxicity results of the variable concentration of compound **1** and **2** (0–80 μg/mL) loaded F-127 NPs. The cell viabilities remained ~80% upon incubation with NPs at 80 μg/mL, indicating that this probe has low cytotoxicity and is suited for biological imaging.

3.5. In vitro cellular imaging

Compound **1** and **2** loaded F-127 NPs are expected to be good candidates for biological imaging due to their suitable size, good stability and good luminescence performance. To evaluate the performance of specific cellular imaging of these NPs, A549 lung cancer cells were chosen for the imaging experiments as target cells. Meanwhile, NIH/3T3 cells were chosen for control experiments. Application of the prepared compound **1** and **2** loaded F-127 NPs in cellular imaging was investigated by confocal laser scanning microscopy (CLSM). A549 cancer cells and 3T3-L1 cells were incubated in culture medium with two NPs suspensions for 4 h at a concentration of 30 μg/mL. The CLSM images of A549 cancer cells after incubation with compound **1** and **2** loaded F-127 NPs are shown in Fig. 7a–c and g–i, respectively. Strong fluorescence could be found in the cytoplasm. Only weak fluorescence could be found in NIH/3T3 cells when the same NPs were incubated (Fig. 7d–f and j–l). Therefore, compound **1** and **2** loaded F-127 NPs are more effectively internalized in the cytoplasm of A549 cancer cells than NIH/3T3 due to the faster endocytosis.

4. Conclusion

In this work, we successfully synthesized four species of FR/NIR organic fluorescent molecules with AIE feature. These fluorophores were assembled into FR/NIR organic fluorescent NPs with the fluorophores as the core and biocompatible F-127 as the encapsulation matrix. It has been showed that the fluorogen-loaded F-127 NPs have small size, strong near-infrared emission and large Stokes shift. These superior performances make the fluorogen-loaded F-127 NPs a potential material in bioimaging. This study provides an efficient strategy to design highly emissive water soluble organic NPs for a wide range of biological detection. Moreover, the developed FR/NIR fluorescent NPs could be further conjugated with specific targeting ligands or functional groups for targeted biological imaging or sensing.

Acknowledgements

This work was supported by (2013CB834701), the Natural Science Foundation of China (No. 51373063, 51573068, 21221063, 21674041) and Program for Chang Jiang Scholars and Innovative Research Team in University (No. IRT101713018) and Program for Changbaishan Scholars of Jilin Province.

Appendix A. Supplementary data

Supplementary data related to this article can be found at http://dx.doi.org/10.1016/j.dyepig.2017.04.004.

References

[1] Newman R, Fosbrink M, Zhang J. Genetically encodable fluorescent biosensors for tracking signaling dynamics in living cells. Chem Rev 2011;111:3614–66.
[2] Borgia1 M, Borgia A, Best R, Steward A, Nettels D, Wunderlich B, et al. Single-molecule fluorescence reveals sequence-specific misfolding in multidomain proteins. Nature 2011;474:662–6.
[3] Bredas J-L, Norton J, Cornil J, Coropceanu V. Molecular understanding of organic solar cells: the challenges. Acc Chem Res 2009;42:1691–9.
[4] Smith A, Duan H Mohs, Nie S. Bioconjugated quantum dots for in vivo molecular and cellular imaging. Adv Drug Deliv Rev 2008;60:1226–40.
[5] Jamieson T, Bakhshi R, Petrova D, Pocock R, Imani M, Seifalian A. Biological applications of quantum dots. Biomaterials 2007;28:4717–32.
[6] Wu W, Chen C, Tian Y, Jang S, Hong Y, Liu Y, et al. Enhancement of aggregation-induced emission in dye-encapsulating polymeric micelles for bioimaging. Adv Funct Mater 2010;20:1413–23.
[7] Hoeben F, Jonkheijm P, Meijer EW, Schenning A. About supramolecular assemblies of π-conjugated systems. Chem Rev 2005;105:1491–684.
[8] Chen Z, Baumeister U, Tschierske C, Würthner F. Effect of core twisting on self-assembly and optical properties of PeryleneBisimide dyes in solution and columnar liquid crystalline phases. Chem Eur J 2007;13:450–65.
[9] Balakrishnan K, Datar A, Naddo T, Huang J, Oitke R, Ma Y, et al. Effect of side-chain substituents on self-assembly of perylene diimide Molecules: morphology control. J Am Chem Soc 2006;128:7390–8.
[10] Huang C, Barlow S, Marder S. Perylene-3,4,9,10-tetracarboxylic acid diimides: synthesis, physical properties, and use in organic electronics. J Org Chem 2011;76:2386–407.
[11] Tang BZ, Zhan X, Yu G, Lee P, Liu Y, Zhu D. Efficient blue emission from siloles. J Mater Chem 2001;11:2974–8.
[12] Luo J, Xie Z, Lam J, Cheng L, Chen H, Qiu C, et al. Aggregation-induced emission of 1-methyl-1,2,3,4,5-pentaphenylsilole. Chem Commun 2001. 1740–1471.
[13] Hong Y, Lam J, Tang B. Aggregation-induced emission: phenomenon, mechanism and applications. Chem Commun 2009:4332–53.
[14] Mahtab F, Yu Y, Lam J, Liu J, Zhang B, Lu P, et al. Fabrication of silica nanoparticles with both efficient fluorescence and strong magnetization and exploration of their biological applications. Adv Funct Mater 2011;21:1733–40.
[15] Li K, Jiang Y, Ding D, Zhang X, Liu Y, Hua J, et al. Folic acid-functionalized two-photon absorbing nanoparticles for targeted MCF-7 cancer cell imaging. Chem Commun 2011;47:7323–5.
[16] An B, Kwon S, Jung S, Park S. Enhanced emission and its switching in fluorescent organic nanoparticles. J Am Chem Soc 2002;124:14410–5.
[17] Guo Z, Shao A, Zhu W. Long wavelength AIEgen of quinoline-malononitrile. J Mater Chem C 2016;4:2640–6.
[18] Shao A, Xie Y, Zhu S. Far-red and near-infrared AIE-active fluorescent organic Nanoprobes with enhanced tumor-targeting efficacy: shape-specific effects. Angew Chem Int Ed 2015;54:7275–80.
[19] Zhao Z, Lu P, Lam J, Wang Z, Chan C, Sung H, et al. Molecular anchors in the solid state: restriction of intramolecular rotation boosts emission efficiency of luminogen aggregates to unity. Chem Sci 2011;2:672–5.
[20] Hong Y, Lam J, Tang B. Aggregation-induced emission. Chem Soc Rev 2011;40:5361–88.
[21] Yuan Y, Zhang C, Gao M, Zhang R, Tang BZ, Liu B. Specific light-up bioprobe with aggregation-induced emission and activatable photoactivity for the targeted and image-guided photodynamic ablation of cancer cells. Angew Chem, Int Ed 2015;54:1780–6.
[22] Zhang R, Yuan Y, Liang J, Kwok R, Zhu Q, Feng G, et al. Fluorogen–peptide conjugates with tunable aggregation-induced emission characteristics for bioprobe design. ACS Appl Mater Interfaces 2014;6:14302–10.
[23] Yuan Y, Kwok R, Feng G, Liang J, Geng J, Tang BZ, et al. Rational design of fluorescent light-up probes based on an AIE luminogen for targeted intracellular thiol imaging. Chem Commun 2014;50:295–7.
[24] Shi H, Kwok R, Liu J, Xing B, Tang BZ, Liu B. Real-time monitoring of cell apoptosis and drug screening using fluorescent light-up probe with aggregation-induced emission characteristics. J Am Chem Soc 2012;134:17972–81.
[25] Shi H, Zhao N, Ding D, Liang J, Tang BZ, Liu B. Fluorescent light-up probe with aggregation-induced emission characteristics for in vivo imaging of cell apoptosis. Org Biomol Chem 2013;11:7289–96.
[26] Liang J, Shi H, Kwok R, Gao M, Yuan Y, Zhang W, et al. Distinct optical and kinetic responses from E/Z isomers of caspase probes with aggregation-induced emission characteristics. J Mater Chem B 2014;2:4363–70.

[27] Ding D, Liang J, Shi H, Kwok R, Gao M, Feng G, et al. Light-up bioprobe with aggregation-induced emission characteristics for real-time apoptosis imaging in target cancer cells. J Mater Chem B 2014;2:231–8.
[28] Yuan Y, Kwok R, Tang BZ, Liu B. Targeted theranostic platinum(IV) prodrug with a built-in aggregation-induced emission light-up apoptosis sensor for noninvasive early evaluation of its therapeutic responses in situ. J Am Chem Soc 2014;136. 2546–2254.
[29] Lu H, Zhao X, Tian W, Wang Q, Shi J. Pluronic F127–folic acid encapsulated nanoparticles with aggregation-induced emission characteristics for targeted cellular imaging. RSC Adv 2014;4:18460–6.
[30] Zhao Q, Li K, Chen S, Qin A, Ding D, Zhang S, et al. Aggregation-induced red-NIR emission organic nanoparticles as effective and photostable fluorescent probes for bioimaging. J Mater Chem 2012;22:15128–35.
[31] Zhao Z, Lam J, Tang BZ. Aggregation-induced emission of tetraarylethene luminogens. Curr Org Chem 2010;14:2109–32.
[32] Zhao Z, Chen B, Geng J, Chang Z, Aparicio-Ixta L, Nie H, et al. Red emissive biocompatible nanoparticles from tetraphenylethene-decorated BODIPY luminogens for two-photon excited fluorescence cellular imaging and mouse brain blood vascular visualization. Part Part Syst Charact 2014;31:481–91.
[33] Liu J, Lam J, Tang BZ. Aggregation-induced emission of silole molecules and polymers: fundamental and applications. J Inorg Organomet Polym Mater 2009;19:249.
[34] Zhao Z, Geng J, Chang Z, Chen S, Deng C, Jiang T, et al. A tetraphenylethene-based red luminophor for an efficient non-doped electroluminescence device and cellular imaging. J Mater Chem 2012;22:11018–21.
[35] Zhao Q, Li K, Chen S, Qin A, Ding D, Zhang S, et al. Aggregation-induced red-NIR emission organic nanoparticles as effective and photostable fluorescent probes for bioimaging. J Mater Chem 2012;22:15128–35.
[36] Zhang X, Zhang X, Wang S, Liu M, Tao L, Wei Y. Surfactant modification of aggregation-induced emission material as biocompatible nanoparticles: facile preparation and cell imaging. Nanoscale 2013;5:147–50.
[37] Wang Z, Yan L, Zhang L, Chen Y, Li H, Zhang J, et al. Ultra bright red AIE dots for cytoplasm and nuclear imaging. Polym Chem 2014;5:7013–20.
[38] Zhang Y, Chang K, Xu B, Chen J, Yan L, Ma S, et al. Highly efficient near-infrared organic dots based on novel AEE fluorogen for specific cancer cell imaging. RSC Adv 2015;5:36837–44.
[39] Lu H, Zheng Y, Zhao X, Wang L, Ma S, Han X, et al. Highly efficient far red/near-infrared solid fluorophores: aggregation-induced emission, intramolecular charge transfer, twisted molecular conformation, and bioimaging applications. Angew Chem, Int Ed 2016;128:163–7.
[40] Qin W, Li K, Feng G, Li M, Yang Z, Liu B, et al. Bright and photostable organic fluorescent dots with aggregation-induced emission characteristics for noninvasive long-term cell imaging. Adv Funct Mater 2014;24:635–43.
[41] Li K, Qin W, Ding D, Tomczak N, Geng J, Liu R, et al. Photostable fluorescent organic dots with aggregation-induced emission (AIE dots) for noninvasive long-term cell tracing. Sci Rep 2013;3:1150.